batteries

MDPI

Article

High Performance H_2−Mn Regenerative Fuel Cells through an Improved Positive Electrode Morphology

Javier Rubio-Garcia [1,2,*], Anthony Kucernak [2,3,*], Barun Kumar Chakrabarti [4], Dong Zhao [2], Danlei Li [2], Yuchen Tang [2], Mengzheng Ouyang [5], Chee Tong John Low [4] and Nigel Brandon [3,5]

1 Department of Materials Science and Metallurgy, University of Cambridge, Cambridge CB2 1TN, UK
2 Department of Chemistry, Faculty of Science, Imperial College London, South Kensington, London SW7 2AZ, UK
3 RFC Power Ltd., London SW7 2PG, UK
4 WMG, Warwick Electrochemical Engineering Group, Energy Innovation Centre, University of Warwick, Coventry CV4 7AL, UK
5 Department of Earth Science and Engineering, Imperial College London, South Kensington, London SW7 2AZ, UK
* Correspondence: jr873@cam.ac.uk (J.R.-G.); anthony@imperial.ac.uk (A.K.)

Abstract: The effective scaling-up of redox flow batteries (RFBs) can be facilitated upon lowering the capital costs. The application of ubiquitous manganese along with hydrogen (known as H_2−Mn regenerative fuel cells (RFC)) is seen as an effective solution for this purpose. Here, we aim to evaluate different positive electrodes so as to improve the key performance metrics of the H_2/Mn RFC, namely electrolyte utilization, energy efficiency, and peak power densities. Commercially available carbon paper and graphite felt are used to show that the latter provides better key performance indicators (KPIs), which is consistent with the results reported for standard all-vanadium RFBs in the literature. Even better KPIs are obtained when an in-house carbon catalyst layer (CCL) is employed in combination with graphite felt electrodes (e.g., more than 80% energy efficiency, >0.5 W cm^{-2} peak power density and electrolyte utilization of 20 Ah L^{-1} for felt and carbon metal fabric (CMF), prepared by means of electrospinning and carbonization, in comparison with about 75% energy efficiency 0.45 W cm^{-2} peak power density and 11 Ah L^{-1} electrolyte utilization for felt on its own). It is envisaged that if the electrochemical performance of CCLs can be optimized then it could open up new opportunities for the commercial exploitation of H_2−Mn systems.

Keywords: redox flow battery; regenerative fuel cell; hydrogen; manganese; electrodes; electrospinning

Citation: Rubio-Garcia, J.; Kucernak, A.; Chakrabarti, B.K.; Zhao, D.; Li, D.; Tang, Y.; Ouyang, M.; Low, C.T.J.; Brandon, N. High Performance H_2−Mn Regenerative Fuel Cells through an Improved Positive Electrode Morphology. *Batteries* **2023**, *9*, 108. https://doi.org/10.3390/batteries9020108

Academic Editors: Pascal Venet and Carlos Ziebert

Received: 5 December 2022
Revised: 19 January 2023
Accepted: 25 January 2023
Published: 3 February 2023

1. Introduction

The deployment of grid-scale energy storage is predominantly constrained by cost, which is a function of the number of hours of storage and, to a lesser extent, the power output. Redox flow batteries (RFBs) can offer exceptional engineering flexibility due to their ability to independently scale power and their energy capacity [1,2]. The former is directly affected by the dimensions of the electrode stack, while the latter is a function of the electrolyte volume. Investigations into improving electrode performance are essential because improving the operational current density while maintaining high electrolyte utilization means lowering the levelized cost of storage [3,4]. For cost-effectiveness and maximizing the benefits of RFBs, electrodes are engineered to tune their microstructural features and chemical stability, so they are suitable for operation under extreme pH conditions [5].

Most RFB redox reactions are outer-sphere processes that can be catalyzed on carbon-based materials. As a result, the performance of the electrode is dictated by its microstructure, porosity, and surface chemistry [3]. The optimization of these parameters results in an impact on different properties such as: (i) pressure drop and mass transport distribution, (ii) wetting properties and electrochemical surface area (ECSA), (iii) heat and

charge transport, and (iv) electrical conductivity or (v) mechanical stability under compression [6]. State-of-the-art RFB electrodes are essentially fibrous carbon-based materials, such as papers [7], cloths, or felts [3], employed particularly in the commercially exploited all-vanadium RFB (VRFB) [8]. However, these carbon-fiber materials do not function optimally in standard aqueous RFB systems, requiring thermal or chemical processes for activation as a means to improve their performances [3]. Various strategies have been employed, especially for VRFBs [9], which include thermal treatment [10], acidic activation [11], sputtering with nanomaterials [12], and plasma activation [13], to name a few [14]. While these processes do not provide significant changes in the microstructure of the material, they contribute to higher accessible ECSA [15]. In this context, we recently introduced the concept of a "carbon catalyst layer" (CCL) by establishing an analogy with the membrane electrode assembly employed in low temperate fuel cells [16]. For RFBs, the CCL term refers to a high surface area carbon material that cannot be directly used as a free-standing electrode material because of its poor mechanical properties, but it can deliver high power output and electrolyte utilization when cushioned between standard and untreated electrode materials such as carbon paper or graphite felt [17]. These CCLs can be fabricated by advanced processes such as screen printing [18] or electrodeposition [19]. In this respect, electrospinning is a strong contender because of its scalability, as well as versatility in terms of fiber dimensions and adaptability to enable 3D structuring. Electrospinning has been applied successfully for preparing membranes and electrodes for energy conversion [20] and storage in recent times [21]. This procedure was used to prepare electrode templates with three different metallic precursors followed by carbonization in order to make carbon metal fabric electrodes [22]. These CCL-based electrodes perform very well in zinc air batteries and have thus aroused interest for application in RFBs. A CCL-analogous material was very recently successfully applied as a positive electrode catalyst in a hydrogen/vanadium hybrid flow battery, and it displayed an improved performance when compared to a standard commercially sourced carbon cloth electrode [17]. This study also encompassed the benefits of a gas−liquid hybrid RFB configuration (also known as a regenerative fuel cell) when compared with the traditional liquid−liquid VRFB cell architecture. Replacing the negative vanadium electrolyte with highly reversible and kinetically fast hydrogen reactions endows a plethora of advantages, including the following: (i) simpler and efficient rebalancing of the electrolyte, as the gas phase cannot be "contaminated" by the liquid catholyte (and vice-versa), and (ii) high power output and efficiency because of the fast kinetics for the hydrogen evolution reaction (HER) and hydrogen oxidation reaction (HOR) on the transition metal catalysts [23].

Several positive liquid electrolytes have been studied in a hybrid RFB configuration, but the use of Br_2-based catholytes has received more attention owing to its advantages in terms of cost, efficiency, power output [24], and resource availability [25]. However, HBr and Br_2 are highly corrosive and toxic compounds (permitted exposure limit time weighted average of gases are 3 ppm and 0.1 ppm respectively) [26] and liquid crossover to the gas side leads to irreversible degradation of the HER/HOR catalyst due to corrosion and poisoning reactions [5,27]. These issues can be solved by using other liquid electrolyte formulations such as those involving V or Ce instead of Br [28]. Manganese is an abundant and inexpensive element that is widely used in disposable alkaline batteries [29]. However, it has hitherto not been explored much for redox flow batteries due to the instability of Mn(III) in aqueous electrolytes, leading to the precipitation of MnO_2 via a disproportionation reaction. The introduction of metal additives within the Mn-electrolyte formulation was recently proposed as a potential strategy to avoid capacity decay due to insoluble MnO_2 formation [30]. This enabled us to demonstrate the first hydrogen/manganese hybrid RFB, showing a very promising performance and projected cost [31]. In this work, we investigate the influence of the carbon positive electrode microstructure on the performance of this system. For this purpose, a selection of commercially available materials was compared with a CCL-homemade electrode synthesized by means of electrospinning. Interestingly, a

significant increase in energy efficiency (EE) to values above 85% at 100 mA cm^{-2} and very high electrolyte utilization (in excess of 90%) was evidenced for the CCL material.

2. Experimental

2.1. Chemicals

Titanium (IV) oxysulfate ($TiOSO_4.xH_2O$) (Sigma-Aldrich, Dorset, (UK), ≥29% Ti), H_2SO_4 (VWR, Lutterworth (UK), 95%), and $MnCO_3$ (Sigma-Aldrich, Dorset, (UK), ≥99.9% trace metal basis) were used as received, and N,N′-dimethylformamide (DMF, Sigma-Aldrich, Dorset, (UK), Technical grade for electrospinning, ~94% pure) was purchased from VWR International. PAN powder was purchased from Goodfellow Cambridge Limited Huntingdon (Huntingdon (UK), average particle size ~50 µm, molecular weight ~230,000 g mol^{-1}). Iron(III) acetylacetonate $Fe(acac)_3$ was bought from Sigma-Aldrich, Dorset, (UK), (≥97%).

2.2. Membrane Electrode Assembly (MEA)

The choice of MEA materials was based on their performance, which was tested and reported in a previous work [17]. The following MEA components were used: (i) gas half-cell (anode): hydrogen electrode with 0.3 mg-Pt cm^{-2} and 40% PTFE loading; (ii) proton exchange membrane: Nafion 117; and (iii) electrolyte half-cell (cathode): carbon paper (SGL group, Meitingen (Germany), Sigracet SGL 10AA), which was used for some testing in the H/Mn RFB followed by 4.6 mm thick untreated graphite felts (SGL group, Meitingen (Germany), Sigracell GFD 4.6 EA), which led to the application of carbon metal fabric (CMF) of 100 µm thickness that was sandwiched with graphite felts and used as the positive electrode.

Nafion membranes were initially cut and activated as reported elsewhere [23]. For cleaning purposes, the membrane was soaked in 1 M hydrogen peroxide (VWR, 30% (W/V)) solution and heated at 80 °C for 1 h. This was followed by rinsing the membrane with deionized water and heating it in 1 M H_2SO_4 (VWR, 95%) solution at 80 °C for 1 h. Finally, it was rinsed and left in deionized water for future use.

The electrolyte preparation and final elemental composition also followed the procedure explained previously [31], where an electrolyte with 1 M Mn and 1 M Ti in 3 M sulfuric acid was produced. Accordingly, when a new electrolyte was prepared, it was allowed to flow through the cell at zero load for about an hour, as reported in an earlier work on regenerative fuel cells [23].

2.3. Electrospinning and Carbonization

To prepare the electrodes, $Fe(acac)_3$ powder was added in ratios ranging 30 wt.% relative to PAN, and it was mixed for 24 h at 55 °C as described elsewhere [17]. The as-prepared precursor solution was then transferred to a syringe and driven into the electrospinning needle at 1.5 mL h^{-1} by a syringe pump integrated in an electrospinning machine (Bioinicia LE-50). High voltages of 10 to 15 kV were applied onto the needle (25 mm length, 20 G) to extract the fiber at a stable rate, with a working distance of 15 cm from the grounded rotating collector, which were tightly covered by a layer of Al foil, and with a rotating speed of 1500 rpm. The electrospinning was done at 25 °C, and at 50% humidity. The as-prepared free-standing nanofiber film was peeled off from the Al collector for subsequent heat treatment. The electrospun fiber mats were calcined in air at 280 °C for 2 h for the stabilization process, followed by a pyrolysis step at 850 °C in nitrogen (N_2) with a 2 °C min ramp rate, so as to initiate the formation of Fe_2O_3 nanoparticles and the nano-CMF "hair-like" structures.

2.4. Redox Flow Battery Cell Assembly

The performance of the H_2-Mn RFB system was determined using a 5 cm^2 active area single cell assembly reported in our previous work [17]. The fuel cell fixture was provided by Scribner Associates. The serpentine flow field for both the positive and negative half-cells

is made of POCO graphite, which is highly chemically resistant. The serpentine flow field provides an improved mass transport rate, which results in a higher operational current density when compared with the standard electrolyte flow through configuration [32]. The outer thin plate is a gold-plated copper current collector that can minimize IR loss (due to the ohmic resistance of the cell). The end plates are anodized aluminum with reactant input and output ports, stainless steel Swagelok compression fittings, cartridge heaters, and thermocouple wells. In order to have a good sealing and balance the pressure distribution, PTFE (Polytetrafluoroethylene) papers that have a high chemical resistance were sandwiched between the MEA as gaskets. The normal compression factor is 75%. A peristaltic pump (Masterflex easy-load) and Masterflex platinum-cured silicone tubing (L/S 14, 25 ft) were used to pump the manganese electrolyte through the cell at flow rates of 25–100 mL min^{-1}. A magnetic stirrer was employed to keep the electrolyte concentration homogeneous. Hydrogen gas, passing through the anode side, was controlled with mass flow regulators at a flow rate of 25–150 mL min^{-1}.

2.5. Charge−Discharge Experiments

Galvanostatic charge and discharge experiments were conducted with a Gamry 3000 potentiostat. To determine the energy, voltage, and coulombic efficiency of the electrochemical cell, all the charge and discharge cycles were performed at a constant current (galvanostatic), whereby a minimum of 10 cycles were carried out at 20, 40, 60, 80, and 100 mA cm^{-2}. Higher current density charging up to 150 mA cm^{-2} was only tested for a combination of graphite felt and CMF as positive electrodes in the H_2−Mn system. Long term charge and discharge efficiencies were determined for a maximum of 100 cycles comparing graphite felt with CMF attached to the felt. In order to avoid producing MnO_2, a cut off voltage of 1.65 V was set as the upper limit. Therefore, once the voltage of the cell reached this value, the power source would stop supplying current. A lower limit of 0.60 V was also introduced as the cut-off voltage for discharge. Power curves were obtained utilizing a Scribner 850e RFB station with the following conditions: (i) constant current 20 mA cm^{-2} increments; (ii) at each current density, the current was held for 20 s, whereby high frequency resistance (HFR) values were recorded at each current; (iii) a resting period of 120 s was allowed between each current increment; and (iv) these steps were carried out until the overpotential reached the cut-off voltage.

3. Results and Discussion

3.1. Morphological Characterization of Electrodes

High-resolution SEM of the carbon paper CCL and graphite felt was performed and is shown in Figure 1. It is noted that carbon paper is highly porous and has a complex three-dimensional structure of carbon fibers interwoven with one another and bound by a carbon-based material (nodes) that appear as multi-layered graphite-like flakes [12]. The SEM image of graphite felt is shown in Figure 1 (left), which indicates a smooth and clean surface, as expected [33]. Felts are widely applied as electrode materials for VRFBs owing to their great stability and high conductivity under concentrated acidic conditions [33]. Their catalytic activity is restricted by the relatively low specific surface area. Thus, various treatments are utilized to modify felts to enhance the redox process via promoting active sites and/or enhancing liquid permeation and wettability. In this respect, most carbon-based catalyst materials have good electronic conductivity and a high specific surface area, such as carbon nanotubes (CNTs). This explains one of the key reasons for using a nanotube-based CCLs in combination with graphite felts as electrodes in this work. Figure 1 (right) shows the SEM image of a hierarchically designed CCL for use as an electrode. In the CCL, the random fiber alignment (non-woven) in the fabric and the presence of hair-like CNTs covering the surface of fibers can be observed. The micron-sized (~0.5 μm) fibers act as a scaffold, while the hair-like structure provides interconnectivities for potentially better electron transfer [22]. The CNTs covering the surface of fibers bear catalytic nanoparticles (Fe) and the encased catalyst nanoparticles can be observed at the tip

of CNTs as well as embedded in carbon fibers. However, the stability of the Fe deposits in the acidic electrolyte (3 M H_2SO_4) will be limited. As a result, the material electrocatalytic performance can be solely ascribed to the carbon surface, which is significantly improved due to the presence of CNTs. This is also supported by our previous work [17] in which the capacitance of different electrodes and a CCL was investigated in pure sulfuric acid solutions, showing a significant improvement in the ECSA for the CCL- sample when compared with commercially available RFB electrodes.

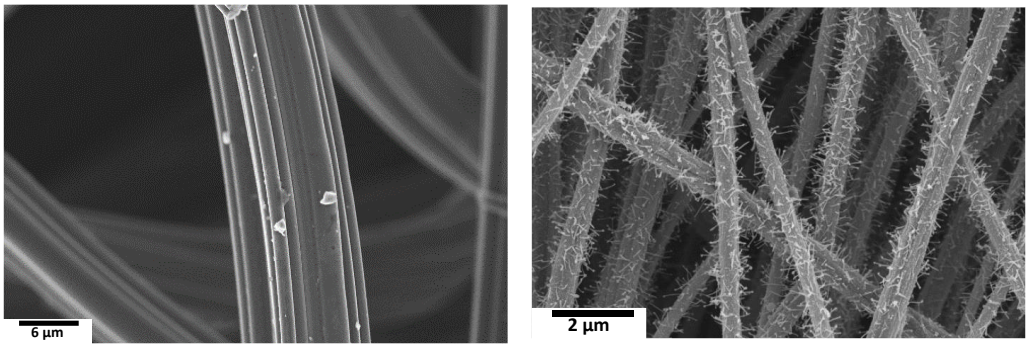

Figure 1. (**Left**) High resolution SEM of graphite felt. (**Right**) High resolution SEM of CCL.

3.2. Single Carbon Paper Electrodes

In a hybrid H_2-Mn (H/Mn) RFB cell, the positive cell reaction is

$$Mn^{2+} \underset{\text{discharge}}{\overset{\text{charge}}{\rightleftarrows}} Mn^{3+} + e^- \quad (1)$$

with simultaneous H^+ transport across the membrane and HER at the negative electrode:

$$2H^+ + 2e^- \underset{\text{discharge}}{\overset{\text{charge}}{\rightleftarrows}} H_2 \quad (2)$$

The opposite processes occur during cell discharge with the oxidation of H_2 to H^+ (HOR) and the reduction of Mn(III) to Mn(II) [31].

Figure 2A displays the H/Mn RFB performance for a single carbon paper ((CP) SGL group, Meitingen (Germany), Sigracet SGL 10AA) electrode on the manganese half-cell. It can be seen that when the current density increased, the capacity of the cell decreased. To facilitate the interpretation of the experimental data, a negative electrode with a high Pt loading (0.3 mg_{Pt} cm^{-2}) in conjunction with a high gas stoichiometry and low operational current density was utilized. This allows for reducing the overpotential at the negative electrode during the charge and discharge (HER and HOR, respectively) to almost negligible values. Under these conditions, it would be fair to assume that Pt can act as a pseudo-reference electrode and the performance of the cell can be thus be dominated by the phenomena taking place at the positive electrode.

At 10 mA cm^{-2}, the average discharged capacity was approximately 95.6% of the theoretical capacity. At 15 and 20 mA cm^{-2}, these values fell to 87% and 84%, respectively, but when the current density continuously rose, at 30 mA cm^{-2} and 40 mA cm^{-2}, the capacity values decreased to 66% and 56%, respectively, of the theoretical value. This occurred due to the activation and concentration overpotentials, as a consequence of the increased chemical reaction rate and rate of ion transport during the charging process. The increased activation overpotential is associated with the greater potential difference between the charge and discharge curves (along with increased ohmic losses). At higher capacity values, the Mn^{2+} concentration dropped below a limiting value and the ion concentration on the cathode was not sufficient enough to generate products at a high rate

due to the increase in the mass transport overpotential. This caused the RFB to reach the upper limit voltage quickly and thus achieve a rather low capacity.

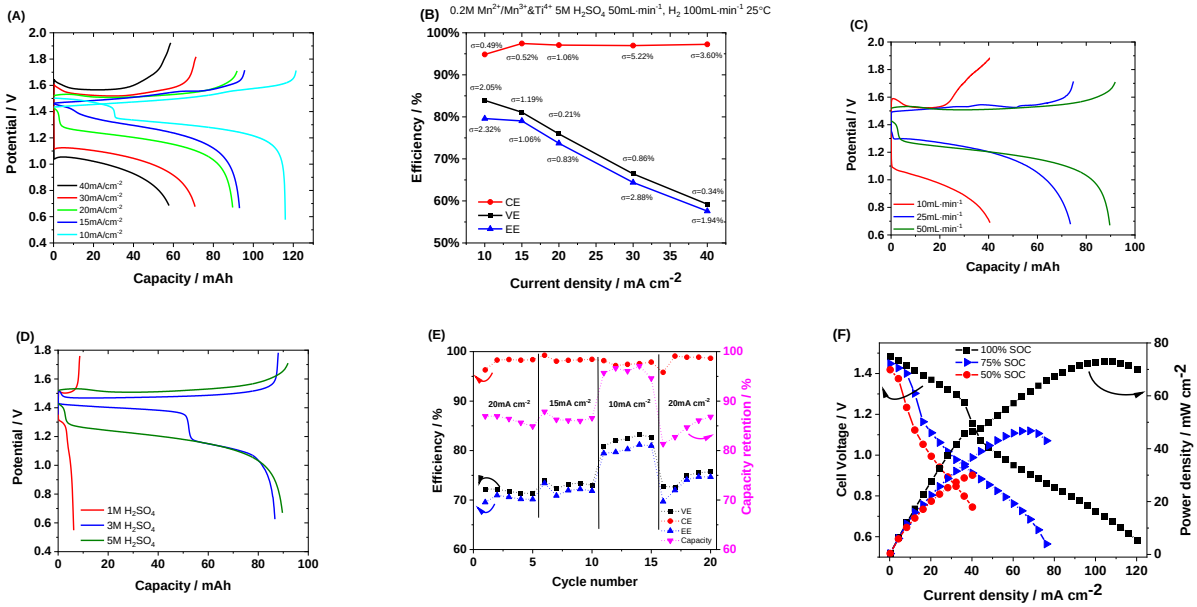

Figure 2. (**A**) Galvanostatic charge and discharge at different current densities with a single layer SGL carbon paper as a positive electrode: 10, 15, 20, 30, and 40 mA cm^{-2}. (**B**) CE, VE, and EE average values over five cycles at different current densities, including standard deviation, to show variability between cycles. (**C**) Galvanostatic charge and discharge at different manganese electrolyte flow rates with a single layer SGL carbon paper as a positive electrode at 50 mA cm^{-2}. (**D**) Galvanostatic charge and discharge at different supporting electrolyte concentration with a single layer SGL carbon paper as a positive electrode at 50 mA cm^{-2}. (**E**) CE, VE, and EE average values over 15 cycles at different current densities (capacity utilization is also displayed). (**F**) Polarization and power density curves at a range of different states-of-charge (SOC). The electrolyte used was 1 M $MnSO_4$, and 1 M $TiOSO_4$ in 3 M H_2SO_4. Hydrogen flow rate = 50 mL min^{-1}, except where stated.

Figure 2B shows the efficiencies of the H/Mn RFB as a function of the different current densities applied (utilizing one positive CP electrode). The CE (Columbic efficiency), which is defined as the ratio of the discharge capacity over the charge capacity, in this system, always remained at a high value of 97% other than a slight dip to 95% at 10 mA cm^{-2}. This suggests that the addition of titanium salt addressed the issue associated with MnO_2 precipitation, which has been discussed in detail in our earlier publication [31]. The high CE may also have had a small contribution from side reactions such as oxygen evolution. It is also noted that when the current density went beyond 30 mA cm^{-2}, despite the CE maintaining a high value, the standard deviation increased. Such capacity decay happens upon cycling and may be associated with side reactions such as oxygen evolution (noting that carbon electrodes are not good catalysts for the oxygen evolution reaction) and carbon oxidation at a high potential (i.e., carbon electrode corrosion around 1.8 V). The VE (voltage efficiency, defined as the average voltage during discharge over the average voltage during charge) were 83.9%, 81.1%, 75.9%, 66.4%, and 59.2% corresponding to 10, 15, 20, 30, and 40 mA cm^{-2}, showing a gradual drop with an increase in the current density values. In addition, from Figure 2A, the charge voltage keeps increasing while the discharge voltage goes lower as a function of the current density increasing. The EE (electrical or energy efficiency, defined as the useful power output divided by total power input, and the product of CE and VE) nearly reached 80% at 10 and 15 mA cm^{-2}, which is better than the literature reported value of 62.7% [34]. In addition, during cell discharge at the lower current density of 10 mA cm^{-2}, a two-step process is involved, the first one being limited at 1.45 V, while the second one was associated with a voltage of 1.2 V. This fact was also noticed in a previous

H/Mn report [31]. The phenomenon was observed regardless of the electrode combination used at the positive side, and thus cannot be attributed to unidentified chemical reactions. We further investigated this and hypothesized that the adsorption/desorption of metal species on the catalyst at the gas side electrode which occur upon liquid crossover caused this phenomenon. This yields variation in the overpotential similar to those commonly reported for soluble lead RFBs, and may be associated with the formation of insoluble species at the electrode that subsequently dissolve [3]. This mechanism is known as charge and discharge "coup de fouet" and could be occurring in the hybrid RFB, although in this case it was the HOR/HER that was affected.

Cell operation was investigated for different liquid electrolyte flow rates and their effects on H/Mn cell capacity is displayed in Figure 2C. During battery charge at 10 mL min^{-1} (red), a sharp increase in cell voltage was evidenced as the SoC increased. This is associated with the direct oxidation of Mn^{2+} directly to MnO_2. Interestingly, the metal oxide can remain soluble when metal additives such as Ti are introduced to the formulation. This means that Mn(IV) can be reversible reduced back to Mn(II) during battery discharge, provided the cell is not left fully charged for lengthy periods. While a high voltage charge could represent a suitable protocol to reach additional capacity (beyond a obe-electron reaction), it promotes the quick degradation of the positive electrode via carbon corrosion. As a consequence, an optimized testing protocol restricting the charge cut-off voltage to <1.7 V was implemented in our experiments.

Increasing the electrolyte velocities through the RFB led to the improved mass transport of manganese ions to the electrode surfaces, and this consequently reduced the diffusion layer thickness. Therefore, the cell capacity was enhanced by increasing the flow rate of the electrolyte. However, this also had an adverse effect of increasing the pressure drop, which adversely impacted the pumping energy requirements, and for this reason, the electrolyte flow was investigated resulting in the best cell performance at 50 mL min^{-1}. We similarly investigated the influence of electrolyte formulations in terms of the supporting electrolyte concentration (H_2SO_4)—Figure 2D. During the charging process, Mn(III) is produced and in an aqueous environment this species goes through a disproportionation reaction to yield soluble Mn(II) and MnO_2 as the precipitate (Equation (3)) [31]. Although a high proton concentration enables better stability, this is offset by increasing the sulphate ion concentrations, which could increase viscosity and thus lower the voltaic efficiencies. Thus, a balance between proton and sulphate ion concentrations is required for a good H/Mn performance. In a 5 cm^2 active area cell we found the best operating conditions and electrolyte stability using a 50 mL min^{-1} flow rate for both gas and liquid sides, 1 M concentration of Mn and Ti, and 3 M of supporting electrolyte.

$$2Mn^{3+} + 2H_2O \rightarrow MnO_2 + Mn^{2+} + 4H^+ \quad (3)$$

Figure 2E displays efficiencies up to 20 cycles at varying current density values for the H/Mn system. The capacity retention is defined as the utilization of the electrical potential, calculated as the discharge capacity divided by the theoretical capacity. After running 20 cycles, the efficiency and capacity were stable and maintained at a good value range. The CE was highly constant at around 98%. It is worth mentioning that upon comparing the 1st–5th cycles with the 16th–20th cycles, which were operated at the same conditions, the voltage efficiency as well as electrical efficiency seemed to improve with the cycles (average VE from 71.8% to 74.3%, EE from 70.3% to 73.0%, respectively). The reason for this may be because the cathode electrode is initially a hydrophobic carbon paper. Therefore, the initial wetting of the electrode was not good, but while running the charge-discharge test at low current densities, some oxygen evolution and carbon oxidation side reactions occurred without damaging the electrode. On the contrary, some formations of carbonyl and carboxyl functional groups could enhance the hydrophilic characteristics and thus lower the internal resistances, resulting in higher voltage efficiencies [35]. In summary, because of the relatively low electrochemical surface area, the operating current density was quite low (20 mA cm^{-2}) and could not be used at a commercialized scale. It

is noted that despite the current density being above 100 mA cm^{-2} for the peak power density (Figure 2F), for a good RFB performance, high round trip efficiency and electrolyte utilization are required. Although power curves are useful to identify losses, it would be unwise to operate the cell at the peak power point, as this is typically associated with a low overall efficiency and electrolyte utilization [3]. Additionally, using a single carbon paper layer leads to a peak power density that can be considered low when compared with other state-of-the-art H/Mn systems that used nitrogen doped graphene as electro-catalysts deposited onto the surfaces of the carbon paper electrodes [23].

According to Houser, a larger electrode thickness causes a higher electrical efficiency, larger capacity, and current density [36]. While a larger electrode thickness increases cell repeat distance and thus decreases volumetric power density, it also results in a reduction in pressure drop that enhances electrolyte convection into the electrode. This causes larger electrolyte volume to flow into the electrode, without allowing the average electrolyte velocity to fluctuate. Thus, three layers of carbon electrode for the cathode side are employed as this would ensure a better residence time of manganese electrolyte in the electrode, allowing improved performances to be ascertained. Figure 3A illustrates the benefits of increasing the positive electrode thickness with successful operation at 100 mA cm^{-2} as a result of improved fluid distribution and lower mass transport overpotential. In alignment with this, it is worth mentioning that an even better performance was observed in our previous work when implementing thick graphite felt (4.6 mm). This is also validated in Figure 3B (green), which shows the performance of an H/Mn system that utilized unmodified graphite felt as a positive electrode. Besides differences in the microstructure, the SGL carbon paper has a significant amount of rough graphitic binder, which could be a residual product of the electrode carbonization process [12], and this binder occupies a large fraction of the microscale pores that partially covers the carbon fibers [37]. In contrast, the felt electrode is binder-free, realizing structural integrity through fiber entanglement, which enables a flexible and compressible media. Therefore, felt allows for better electrolyte permeation to the graphite fiber surfaces, allowing for good mass transport. In full scale systems, graphite felts are preferable as electrodes owing to their electrical resistivity being lower than carbon paper, but more importantly due to their cost, which is between 2 to 10 times less than standard carbon paper electrodes.

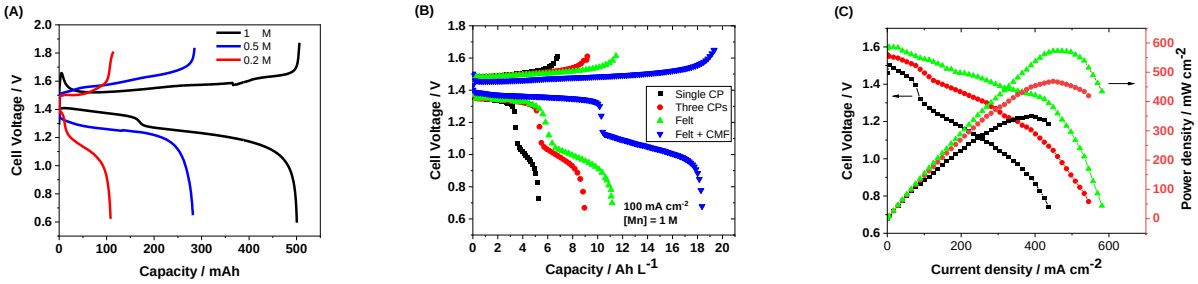

Figure 3. (**A**) Galvanostatic charge and discharge of three carbon paper (CP) electrodes in H/Mn for different manganese electrolyte concentrations. 0.2 M (red), 0.5 M (blue) and 1 M (black). (**B**) H/Mn RFB capacity over five cycles for carbon paper electrodes (one (black) and three layers (red)) compared with a single graphite felt electrode (green). Additionally, the cell capacities are compared with that using a single graphite felt combined with a single CMF as the positive electrode (blue). The electrolyte used was 1 M $MnSO_4$, and 1 M $TiOSO_4$ in 3 M H_2SO_4. Hydrogen flow rate = 50 mL min^{-1}, except where stated. (**C**) H/Mn polarization and power density curves for CP (black), felt (red), and CMF + felt (green) positive electrodes.

Remarkably, when one layer of CMF is placed between the graphite felt and the Nafion membrane, the H/Mn RFB capacity increases by about 1.5 times (Figure 3B). Whereas placing the CMF layer directly in touch with the membrane contributes to reducing the ohmic drop, the operational current density of the H/Mn system is relatively low, and the ameliorated battery performance cannot be attributed to ohmic losses. This is also sup-

ported by Figure 3C with a peak power for the unmodified graphite felt of 470 mW cm^{-2} at 1.05 V (red). The introduction of CCL leads to a 17.5% peak power increase up to 570 mW cm^{-2} at 1.24 V (green). These results are in alignment with our observations for graphene oxide CCLs [5]. The improved performances here are attributed to the CCL possessing micron-sized (~0.5 µm) fibers that behave akin to hair-like structures that provide interconnectivities, increase the surface area, and increase the mechanical robustness of the fabrics. The CNTs covering the surface of the fibers embedded in carbon fibers provide not only a high ECSA, but also good wettability for the active electrolytes.

It is worth mentioning that the peak power results obtained here are comparable to those reported recently for other gas–liquid RFBs such as hydrogen/bromine [38] and hydrogen/vanadium [17] systems. This is true, despite the fact that the H/Mn system was operated by recirculating the manganese electrolyte in a closed loop, unlike the single liquid flow method for which we reported a peak power density above 1.2 W cm^{-2} [31].

Figure 4A shows the galvanostatic charge and discharge for the CCL-positive electrode at different current densities. Large electrolyte utilization >87% of the theoretical value was achieved at 100 mA cm^{-2} (red). This is noteworthy as the commercially available all-vanadium RFBs normally operate below 120 mA cm^{-2} (commonly 80 mA cm^{-2}) to ensure a high energy efficiency (≈85%) and good electrolyte utilization (>75%) [39]. In terms of capacity and energy density, our manganese system would reach values as high as 24 Wh L^{-1} at 100 mA cm^{-2}, which compares favorably with the current vanadium RFBs that show typical values of 10–15 Wh L^{-1}. We finally investigated the stability of the CCL by extended full charge and discharge cycling at 100 mA cm^{-2}, Figure 4B. A very high EE of above 84% and an excellent capacity retention was observed. This not only indicates CCL stability, but also negates hydrogen reactions as limiting processes in the H/Mn RFB. The incorporation of new CCL structures in the future in conjunction with the development of new porous carbon CCL supports with enhanced fluid distribution will be critical to achieve high performing and inexpensive batteries for medium- to large-scale storage applications.

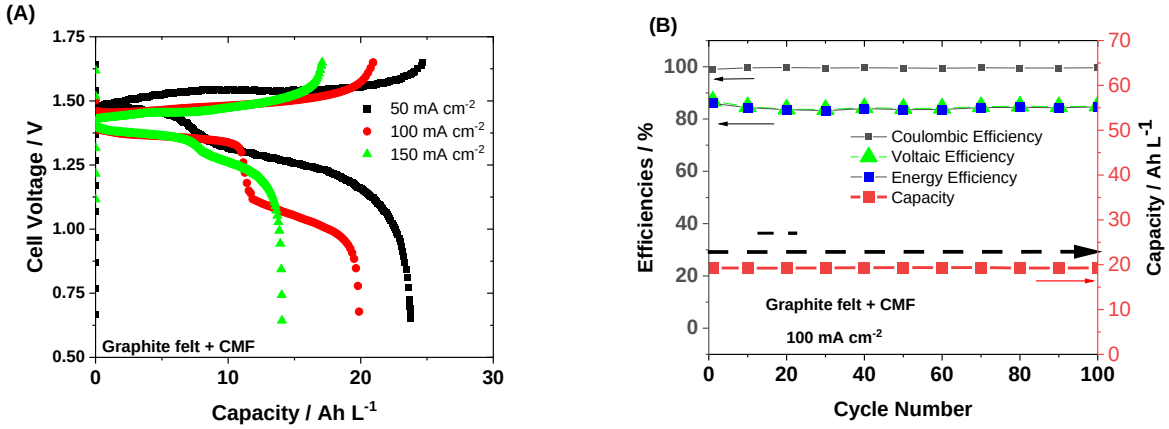

Figure 4. (**A**) Galvanostatic charge and discharge (GCD) at different current densities: 50, 100, and 150 mA cm^{-2}. (**B**) GCD of H/Mn for 100 cycles with efficiencies and electrolyte capacity utilization for CMF and felt. Electrolyte 1 M $MnSO_4$, 1 M $Ti(SO_4)_2$, and 3 M H_2SO_4. Hydrogen 100 mL min^{-1} and liquid flow rate of 50 mL min^{-1}.

In this work, several positive electrodes were employed in the hydrogen/manganese hybrid redox flow battery (regenerative fuel cell). Graphite felt showed a better performance and thus this was used in combination with carbon metal fabrics (also termed carbon catalyst layers) to improve the performance even further. High energy efficiencies in excess of 84% were noted at 100 mA cm^{-2} along with high peak power densities above 0.57 W cm^{-2}. In addition, 100 charge/discharge cycles were successfully performed at the same current density with electrolyte capacities above 20 Wh L^{-1}. Therefore, this

combination of electrodes warrants further investigations in future to optimize the H/Mn system for potential commercial exploitation.

4. Future Perspectives

Carbon-based electrodes have been a strong contender in most RFBs and recently in RFCs, but their drawback lies in the fact that they are mostly sourced from fossil fuel petroleum-based resources. A recent review has highlighted the benefits of sourcing and processing biomass to produce various carbon-based materials, ranging from catalyst to free-standing electrodes for RFBs [40]. It is worth noting that biomass-derived carbon electrodes can also be prepared via electrospinning, as discussed in our current work, and could be of exceptional value for RFBs in the future. Whatever applies for RFBs tends to work equally well with RFCs, except for the gas side half-cell reactions where PEMFC-based gas diffusion carbon electrodes are usually applied. It is anticipated that sustainable sourcing and processing of biomass will be able to replace gas diffusion carbon electrodes for the gas side half-cell in a successful manner.

Author Contributions: J.R.-G. and B.K.C. wrote the manuscript. J.R.-G. and A.K. contributed to the conceptual design. J.R.-G., B.K.C., D.Z., D.L., Y.T. and M.O. contributed to the experimental work. C.T.J.L., N.B. and A.K. contributed to the editing of the manuscript. N.B. and A.K. supervised the work. All authors have read and agreed to the published version of the manuscript.

Funding: This research was funded by Engineering and Physical Sciences, Research Council, under projects with grant numbers EP/K002252/1, EP/L019469/1, EP/N032888/1 and EP/J016454/1.

Data Availability Statement: The data used to produce the figures in this paper is available to download at 10.5281/zenodo.7599405.

Acknowledgments: The authors would like to acknowledge support from the Engineering and Physical Sciences, Research Council.

Conflicts of Interest: A UK patent application has been filed on this specific technology, and US Patent 9391339, "Regenerative fuel cells" covers the general approach.

References

1. Chakrabarti, M.H.; Hajimolana, S.A.; Mjalli, F.S.; Saleem, M.; Mustafa, I. Redox Flow Battery for Energy Storage. *Arab. J. Sci. Eng.* **2013**, *38*, 723–739. [CrossRef]
2. Arenas, L.F.; Ponce de León, C.; Walsh, F.C. Redox flow batteries for energy storage: Their promise, achievements and challenges. *Curr. Opin. Electrochem.* **2019**, *16*, 117–126. [CrossRef]
3. Chakrabarti, B.K.; Kalamaras, E.; Singh, A.K.; Bertei, A.; Rubio-Garcia, J.; Yufit, V.; Tenny, K.M.; Wu, B.; Tariq, F.; Hajimolana, Y.S.; et al. Modelling of redox flow battery electrode processes at a range of length scales: A review. *Sustain. Energy Fuels* **2020**, *4*, 5433–5468. [CrossRef]
4. Gencten, M.; Sahin, Y. A critical review on progress of the electrode materials of vanadium redox flow battery. *Int. J. Energy Res.* **2020**, *44*, 7903–7923. [CrossRef]
5. Chakrabarti, B.; Yufit, V.; Kavei, A.; Xia, Y.; Stevenson, G.; Kalamaras, E.; Luo, H.; Feng, J.; Tariq, F.; Taiwo, O.; et al. Charge/discharge and cycling performance of flexible carbon paper electrodes in a regenerative hydrogen/vanadium fuel cell. *Int. J. Hydrog. Energy* **2019**, *44*, 30093–30107. [CrossRef]
6. Jervis, R.; Kok, M.D.R.; Neville, T.P.; Meyer, Q.; Brown, L.D.; Iacoviello, F.; Gostick, J.T.; Brett, D.J.L.; Shearing, P.R. In situ compression and X-ray computed tomography of flow battery electrodes. *J. Energy Chem.* **2018**, *27*, 1353–1361. [CrossRef]
7. Chakrabarti, B.; Rubio-Garcia, J.; Kalamaras, E.; Yufit, V.; Tariq, F.; Low, C.T.J.; Kucernak, A.; Brandon, N. Evaluation of a Non-Aqueous Vanadium Redox Flow Battery Using a Deep Eutectic Solvent and Graphene-Modified Carbon Electrodes via Electrophoretic Deposition. *Batteries* **2020**, *6*, 38. [CrossRef]
8. Flox, C.; Fàbrega, C.; Andreu, T.; Morata, A.; Skoumal, M.; Rubio-Garcia, J.; Morante, J.R. Highly electrocatalytic flexible nanofiber for improved vanadium-based redox flow battery cathode electrodes. *RSC Adv.* **2013**, *3*, 12056–12059. [CrossRef]
9. Tariq, F.; Rubio-Garcia, J.; Yufit, V.; Bertei, A.; Chakrabarti, B.K.; Kucernak, A.; Brandon, N. Uncovering the mechanisms of electrolyte permeation in porous electrodes for redox flow batteries through real time in situ 3D imaging. *Sustain. Energy Fuels* **2018**, *2*, 2068–2080. [CrossRef]
10. Ghasemiestahbanati, E.; Shaibani, M.; Konstas, K.; Chakrabarti, B.K.; Low, C.T.J.; Majumder, M.; Hill, M.R. Charge Carrier Molecular Sieve (CCMS) Membranes with Anti-aging Effect for Long-Life Vanadium Redox Flow Batteries. *ACS Appl. Energy Mater.* **2022**, *5*, 1505–1515. [CrossRef]

11. Hassan, A.; Tzedakis, T. Facile chemical activation of graphite felt by $KMnO_4$ acidic solution for vanadium redox flow batteries. *Appl. Surf. Sci.* **2020**, *528*, 146808. [CrossRef]
12. Chakrabarti, B.; Nir, D.; Yufit, V.; Tariq, F.; Rubio-Garcia, J.; Maher, R.; Kucernak, A.; Aravind, P.V.; Brandon, N. Performance Enhancement of Reduced Graphene Oxide-Modified Carbon Electrodes for Vanadium Redox-Flow Systems. *ChemElectroChem* **2017**, *4*, 194–200. [CrossRef]
13. Rubio-Garcia, J.; Cui, J.; Parra-Puerto, A.; Kucernak, A. Hydrogen/Vanadium Hybrid Redox Flow Battery with enhanced electrolyte concentration. *Energy Storage Mater.* **2020**, *31*, 1–10. [CrossRef]
14. Chakrabarti, B.K.; Gençten, M.; Bree, G.; Dao, A.H.; Mandler, D.; Low, C.T.J. Modern practices in electrophoretic deposition to manufacture energy storage electrodes. *Int. J. Energy Res.* **2022**, *46*, 13205–13250. [CrossRef]
15. Jacquemond, R.R.; Wan, C.T.-C.; Chiang, Y.-M.; Borneman, Z.; Brushett, F.R.; Nijmeijer, K.; Forner-Cuenca, A. Microstructural engineering of high-power redox flow battery electrodes via non-solvent induced phase separation. *Cell Rep. Phys. Sci.* **2022**, *3*, 100943. [CrossRef]
16. Dai, W.; Wang, H.; Yuan, X.-Z.; Martin, J.J.; Yang, D.; Qiao, J.; Ma, J. A review on water balance in the membrane electrode assembly of proton exchange membrane fuel cells. *Int. J. Hydrog. Energy* **2009**, *34*, 9461–9478. [CrossRef]
17. Chakrabarti, B.K.; Kalamaras, E.; Ouyang, M.; Liu, X.; Remy, G.; Wilson, P.F.; Williams, M.A.; Rubio-Garcia, J.; Yufit, V.; Bree, G.; et al. Trichome-like Carbon-Metal Fabrics Made of Carbon Microfibers, Carbon Nanotubes, and Fe-Based Nanoparticles as Electrodes for Regenerative Hydrogen/Vanadium Flow Cells. *ACS Appl. Nano Mater.* **2021**, *4*, 10754–10763. [CrossRef]
18. Hwang, D.S.; Park, C.H.; Yi, S.C.; Lee, Y.M. Optimal catalyst layer structure of polymer electrolyte membrane fuel cell. *Int. J. Hydrog. Energy* **2011**, *36*, 9876–9885. [CrossRef]
19. Sharma, R.; Kar, K.K. Hierarchically structured catalyst layer for the oxygen reduction reaction fabricated by electrodeposition of platinum on carbon nanotube coated carbon fiber. *RSC Adv.* **2015**, *5*, 66518–66527. [CrossRef]
20. Rajabalizadeh Mojarrad, N.; Iskandarani, B.; Taşdemir, A.; Yürüm, A.; Alkan Gürsel, S.; Yarar Kaplan, B. Nanofiber based hybrid sulfonated silica/P(VDF-TrFE) membranes for PEM fuel cells. *Int. J. Hydrog. Energy* **2021**, *46*, 13583–13593. [CrossRef]
21. Iskandarani, B.; Rajabalizadeh Mojarrad, N.; Yürüm, A.; Alkan Gürsel, S.; Yarar Kaplan, B. Electrospun Nanofiber Electrodes for Boosted Performance and Durability at Lower Humidity Operation of PEM Fuel Cells. *Energy Fuels* **2022**, *36*, 9282–9294. [CrossRef]
22. Liu, X.; Ouyang, M.; Orzech, M.W.; Niu, Y.; Tang, W.; Chen, J.; Marlow, M.N.; Puhan, D.; Zhao, Y.; Tan, R.; et al. In-situ fabrication of carbon-metal fabrics as freestanding electrodes for high-performance flexible energy storage devices. *Energy Storage Mater.* **2020**, *30*, 329–336. [CrossRef]
23. Chakrabarti, B.K.; Feng, J.; Kalamaras, E.; Rubio-Garcia, J.; George, C.; Luo, H.; Xia, Y.; Yufit, V.; Titirici, M.-M.; Low, C.T.J.; et al. Hybrid Redox Flow Cells with Enhanced Electrochemical Performance via Binderless and Electrophoretically Deposited Nitrogen-Doped Graphene on Carbon Paper Electrodes. *ACS Appl. Mater. Interfaces* **2020**, *12*, 53869–53878. [CrossRef]
24. Singh, N.; McFarland, E.W. Levelized cost of energy and sensitivity analysis for the hydrogen–bromine flow battery. *J. Power Sources* **2015**, *288*, 187–198. [CrossRef]
25. Cho, K.T.; Tucker, M.C.; Ding, M.; Ridgway, P.; Battaglia, V.S.; Srinivasan, V.; Weber, A.Z. Cyclic Performance Analysis of Hydrogen/Bromine Flow Batteries for Grid-Scale Energy Storage. *ChemPlusChem* **2015**, *80*, 402–411. [CrossRef]
26. Lyday, P.A. *Bromine*; Bureau of Mines, US Department of the Interior Information: Washington, DC, USA, 1985.
27. Pino-Muñoz, C.A.; Chakrabarti, B.K.; Yufit, V.; Brandon, N.P. Characterization of a Regenerative Hydrogen-Vanadium Fuel Cell Using an Experimentally Validated Unit Cell Model. *J. Electrochem. Soc.* **2019**, *166*, A3511–A3524. [CrossRef]
28. Leung, P.K.; Ponce-de-León, C.; Low, C.T.J.; Shah, A.A.; Walsh, F.C. Characterization of a zinc–cerium flow battery. *J. Power Sources* **2011**, *196*, 5174–5185. [CrossRef]
29. Kordesh, K.; Weissenbacher, M. Rechargeable alkaline manganese dioxide/zinc batteries. *J. Power Sources* **1994**, *51*, 61–78. [CrossRef]
30. Reynard, D.; Maye, S.; Peljo, P.; Chanda, V.; Girault, H.H.; Gentil, S. Vanadium–Manganese Redox Flow Battery: Study of MnIII Disproportionation in the Presence of Other Metallic Ions. *Chem. Eur. J.* **2020**, *26*, 7250–7257. [CrossRef] [PubMed]
31. Rubio-Garcia, J.; Kucernak, A.; Zhao, D.; Li, D.; Fahy, K.; Yufit, V.; Brandon, N.; Gomez-Gonzalez, M. Hydrogen/manganese hybrid redox flow battery. *J. Phys. Energy* **2019**, *1*, 015006. [CrossRef]
32. Liu, H.; Li, P.; Juarez-Robles, D.; Wang, K.; Hernandez-Guerrero, A. Experimental Study and Comparison of Various Designs of Gas Flow Fields to PEM Fuel Cells and Cell Stack Performance. *Front. Energy Res.* **2014**, *2*, 2. [CrossRef]
33. Zhang, L.; Yue, J.; Deng, Q.; Ling, W.; Zhou, C.-J.; Zeng, X.-X.; Zhou, C.; Wu, X.-W.; Wu, Y. Preparation of a porous graphite felt electrode for advance vanadium redox flow batteries. *RSC Adv.* **2020**, *10*, 13374–13378. [CrossRef]
34. Xue, F.-Q.; Wang, Y.-L.; Wang, W.-H.; Wang, X.-D. Investigation on the electrode process of the Mn(II)/Mn(III) couple in redox flow battery. *Electrochim. Acta* **2008**, *53*, 6636–6642. [CrossRef]
35. Jiang, Q.; Ren, Y.; Yang, Y.; Wang, L.; Dai, L.; He, Z. Recent advances in carbon-based electrocatalysts for vanadium redox flow battery: Mechanisms, properties, and perspectives. *Compos. Part B Eng.* **2022**, *242*, 110094. [CrossRef]
36. Houser, J.; Clement, J.; Pezeshki, A.; Mench, M.M. Influence of architecture and material properties on vanadium redox flow battery performance. *J. Power Sources* **2016**, *302*, 369–377. [CrossRef]
37. Forner-Cuenca, A.; Penn, E.E.; Oliveira, A.M.; Brushett, F.R. Exploring the Role of Electrode Microstructure on the Performance of Non-Aqueous Redox Flow Batteries. *J. Electrochem. Soc.* **2019**, *166*, A2230. [CrossRef]

38. Karaeyvaz, M.C.; Duman, B.; Fıçıcılar, B. An alternative HCMS carbon catalyst in bromine reduction reaction for hydrogen-bromine flow batteries. *Int. J. Hydrog. Energy* **2021**, *46*, 29512–29522. [CrossRef]
39. Zheng, Q.; Xing, F.; Li, X.; Liu, T.; Lai, Q.; Ning, G.; Zhang, H. Investigation on the performance evaluation method of flow batteries. *J. Power Sources* **2014**, *266*, 145–149. [CrossRef]
40. Thielke, M.W.; Tian, G.; Sobrido, A.J. Sustainable electrodes for the next generation of redox flow batteries. *J. Phys. Mater.* **2022**, *5*, 024004. [CrossRef]